Time evolution of mixing in heterogeneous porous media

Jean-Raynald de Dreuzy, Jesus Carrera, Marco Dentz, Tanguy Le Borgne

Time evolution of mixing in heterogeneous porous media

J.-R. de Dreuzy,[1,2] J. Carrera,[1] M. Dentz,[1] and T. Le Borgne[2]

Received 6 September 2011; revised 29 March 2012; accepted 28 April 2012; published 12 June 2012.

[1] Mixing in heterogeneous media results from the competition between velocity fluctuations and local scale diffusion. Velocity fluctuations create a potential for mixing by generating disorder and large interfacial areas between resident and invading waters. Local scale diffusion smoothes out the disorder while transforming this potential into effective mixing. The effective mixing state is quantified by the integral of concentration squared over the spatial domain. Because it emerges from dispersion, the potential mixing is defined as the mixing state of a Gaussian plume that has the same longitudinal dispersion as the real plume. The difference γ between effective and potential mixing normalized by the latter traduces the lag of diffusion to homogenize the concentration structure generated by the dispersion processes. This new decomposition of effective mixing into potential mixing and departure rate γ makes a full use of dispersion for quantifying mixing and restricts the analysis of mixing to γ. For cases where the mean concentration can be assumed Gaussian, we use the concentration variance equation of Kapoor and Gelhar (1994) to show that γ depends solely on the macrodispersion coefficient (spreading rate) and the recently developed mixing scale defined as the smallest scale over which concentration can be considered uniform, and which quantifies the internal plume disorder. We use numerical simulations to show that γ turns out to follow a simple scaling form that depends on neither the heterogeneity level or the Peclet number. A very similar scaling form is recovered for Taylor dispersion. Both derivations of γ reinforce its relevance to characterize mixing. This generic characterization of mixing can offer new ways to set up transport equations that honor not only advection and spreading but also mixing.

Citation: de Dreuzy, J.-R., J. Carrera, M. Dentz, and T. Le Borgne (2012), Time evolution of mixing in heterogeneous porous media, *Water Resour. Res.*, *48*, W06511, doi:10.1029/2011WR011360.

1. Introduction

[2] Solute transport has been traditionally described in terms of advection and dispersion. Advection represents the mean displacement of the solute and is expressed in terms of the mean fluid velocity. Dispersion quantifies the rate of spreading of the solute plume and is expressed in terms of the dispersion coefficient. This description is sufficient for many purposes (e.g., risk analysis), but insufficient when mixing-driven chemical reactions come into play. The rate of reaction is often controlled by the rate at which reactants mix. Hence, it is not surprising that mixing has been thoroughly studied in porous media [*Cirpka and Kitanidis*, 2000; *de Simoni et al.*, 2005; *Kitanidis*, 1994] as well as in complex flows [*Pope*, 2000; *Tennekes and Lumley*, 1972].

[3] Assuming that transport is locally Fickian, *de Simoni et al.* [2005] found that the rate of fast reactions is given by $r = f_Q \cdot f_m$, where f_Q is a chemical factor, dependent on reaction parameters, and f_m is a mixing factor given by $\nabla c d_0 \nabla c$ with d_0 the diffusion coefficient and c the local concentration. This expression points out that mixing results from the effect of diffusion. As such, it tends to homogenize concentration distributions. However diffusion alone yields limited mixing. It can however be strongly enhanced by flow heterogeneity that generates complex concentration patterns and increases ∇c [*Chiogna et al.*, 2011; *Le Borgne et al.*, 2010; *Rolle et al.*, 2009; *Tartakovsky et al.*, 2008].

[4] The key question is how to characterize and evaluate mixing. Using the mixing factor f_m, a natural choice for the overall mixing rate is:

$$\chi(t) = \int_\Omega d^d x d_0 \nabla c(\mathbf{x},t) \cdot \nabla c(\mathbf{x},t), \tag{1}$$

where Ω is the overall domain. This magnitude is called scalar dissipation rate because it quantifies the rate of decay of the second moment of concentration $M(t)$ [*Pope*, 2000]. Indeed assuming that concentration obeys the advection diffusion equation and that solute flux through the boundaries is zero, then

$$\chi(t) = -\frac{1}{2}\frac{dM(t)}{dt}, \tag{2}$$

[1]Institute of Environmental Analysis and Water Studies, CSIC, Barcelona, Spain.
[2]Géosciences Rennes, UMR CNRS 6118, Université de Rennes 1, Rennes, France.

Corresponding author: J.-R. de Dreuzy, Institute of Environmental Analysis and Water Studies, CSIC, c/ Jordi Girona, 18-26, 08034 Barcelona, Spain. (jean-raynald.de-dreuzy@univ-rennes1.fr)

0043-1397/12/2011WR011360

where

$$M(t) = \int_{\Omega} d^d x c^2. \tag{3}$$

[5] Therefore, $M(t)$ characterizes a mixing state in the sense that the better mixed, the smaller $M(t)$. It is clear that a proper description of transport should honor not only advection and spreading (dispersion), but also mixing. This work is motivated by the need to find a quantitative evaluation of mixing (i.e., $M(t)$) to test candidate transport equations.

[6] The problem lies in the intricate link between spreading and mixing. In fact, late time mixing rate can be explained in terms of spreading rate [*Le Borgne et al.*, 2010]. This together with the view of local mixing as controlled by diffusion shows that the mixing stat $M(t)$ results from both the local diffusion processes and the more global dispersion processes. Therefore, it is natural to distinguish these two origins of mixing by expressing concentration as the sum of the average concentration $\overline{c}$ and the deviation about it c':

$$c = \overline{c} + c'. \tag{4}$$

[7] Schematically $\overline{c}$ and c' are expected to rate the contributions to mixing of spreading (i.e., dispersion) and diffusion, respectively. More precisely, using equations (3) and (4) and the fact that $\overline{c'} = 0$, the mixing state $M(t)$ can then be decomposed in

$$M(t) = M_1(t) + M_2(t). \tag{5}$$

with

$$M_1(t) = \int_{\Omega} d^d x \overline{c}^2 \tag{6}$$

$$M_2(t) = \int_{\Omega} d^d x c'^2. \tag{7}$$

[8] That is, the overall actual mixing state $M(t)$ is the sum of what we call the dispersive mixing state $M_1(t)$ and the local mixing state $M_2(t)$. For stratified flows, *Bolster et al.* [2011] show that the actual mixing $M(t)$ departs from dispersive mixing, which represents the effect of spreading, at times lower than the diffusion time. At this stage, $M_2(t)$ is significantly larger than 0 showing that concentration perturbations triggered by advective heterogeneities are not yet wiped out by diffusion. Asymptotically however, mixing becomes dominated by spreading and $M(t)$ becomes equal to $M_1(t)$.

[9] The decomposition of mixing given by equation (5) is not only natural, it is also appealing because the local mixing state $M_2(t)$ turns out to be precisely the spatially integrated concentration variance $\|\sigma_c^2\|$, a quantity that has been extensively studied for uncertainty quantification, solute plume characterization and risk analysis to cite only few applications [*Andricevic*, 1998; *Caroni and Fiorotto*, 2005; *Fiori and Dagan*, 2000; *Fiori*, 2001; *Fiorotto and Caroni*, 2002; *Kapoor and Gelhar*, 1994a, 1994b; *Kapoor and Kitanidis*, 1998; *Pannone and Kitanidis*, 1999; *Tennekes and Lumley*, 1972; *Tonina and Bellin*, 2008; *Vanderborght*, 2001]. Unfortunately, although appealing, this decomposition cannot generally be used for relating mixing to spreading because most results on concentration variance are based on the approximation that the mean concentration $\overline{c}$ is Gaussian [*Fiori and Dagan*, 2000; *Kapoor and Gelhar*, 1994a; *Kapoor and Kitanidis*, 1998]. Under this closure assumption, $\overline{c}$ can effectively be derived from spreading. The assumption of Gaussianity is however valid only at late times (i.e., much larger than the advection time) or for low levels of heterogeneity, i.e., in the conditions that have been classically investigated [*Kapoor and Kitanidis*, 1998; *Tonina and Bellin*, 2008; *Vanderborght*, 2001]. Actually, the mean concentration $\overline{c}$ becomes significantly non Gaussian at early times and high heterogeneity (Figure 1). Since most mixing occurs then, it is clear that the deviation of actual from dispersive mixing may play an important role and needs to be studied. The objective of our work is precisely to analyze such deviation so as to propose a quantitative evaluation of the evolution of mixing.

2. Model, Numerical Methods and Computation of Mixing States

[10] As mentioned in the introduction, the decomposition of the actual mixing state $M(t)$ into dispersive and local mixing states, $M_1(t)$ and $M_2(t)$ is not convenient because computation of $M_1(t)$ is not immediate. Instead, we propose decomposition into a potential macrodispersive mixing M_D state and a deviation rate γ, defined as:

$$\gamma(t) = \frac{M(t) - M_D(t)}{M_D(t)}, \tag{8}$$

where $M_D(t)$ is the mixing state corresponding to a Gaussian plume that has the same longitudinal dispersion σ_L as the real plume:

$$M_D(t) = \frac{m_0^2}{2L_2\sqrt{\pi}\sigma_L}. \tag{9}$$

with m_0 the mass of solute initially injected transversally to the main flow direction over a line of length L_2 [*Le Borgne et al.*, 2010]. $M_D(t)$ quantifies the mixing state that corresponds to the maximum entropy that can be achieved for the longitudinal spreading σ_L. Notice that the Gaussian distribution maximizes the concentration entropy for a given mean and dispersion σ_L [*Kitanidis*, 1994]. That is, $M_D(t)$ quantifies the best (i.e., most thoroughly) mixed state that can be achieved for the longitudinal spreading σ_L. The action of local diffusion is indispensable to translate this mixing potential into effective mixing.

[11] γ measures the relative deviation of actual mixing from the potential macrodispersive (Gaussian) mixing state. When it is zero, the whole zone occupied by the plume as measured by the macrodispersion coefficient is well mixed. When it is much larger than zero, the plume is not well mixed within the zone that it occupies. It happens for example at high Peclet number when concentrations are organized around a long folded filament packed in a restricted zone. The full description of the overall mixing state then

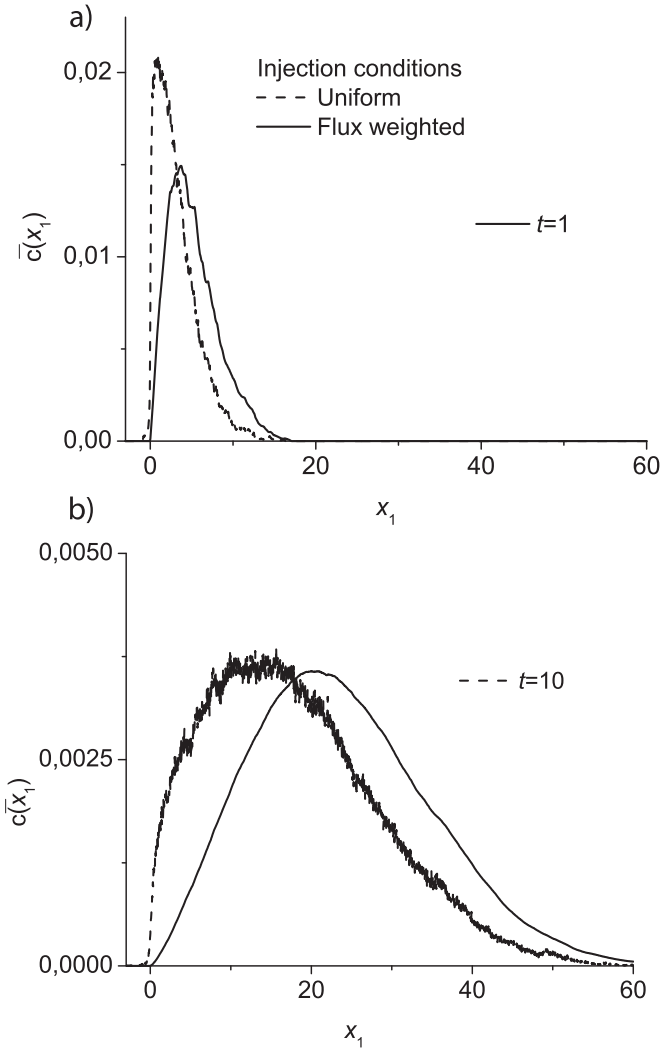

Figure 1. Concentration profiles $\overline{c}(x_1)$ for $Pe = 500$ and $\sigma_Y^2 = 9$ at times equal (a) to the advection time scale ($t = 1$) and (b) to 10 times larger than the advection time scale ($t = 10$). Solute is injected on a long line transversally to the mean flow direction. Injection is either uniform (dashed line) or flux weighted (solid line).

reduces to the characterization of the relative deviation from the potential macrodispersive mixing state, $\gamma(t)$, so that

$$M(t) = M_D(t)\left(1 + \gamma(t)\right). \tag{10}$$

[12] As opposed to the decomposition (5) of $M(t)$ into dispersive and local mixing, this alternative decomposition of $M(t)$ is advantageous for two reasons. First, it makes use of the large body of knowledge available on dispersion for evaluating $M_D(t)$ [*Dagan*, 1989; *de Dreuzy et al.*, 2007; *Dentz et al.*, 2000; *Gelhar and Axness*, 1983; *Gelhar*, 1993; *Neuman and Zhang*, 1990]. Second, it does not require the mean concentration to be Gaussian, as γ contains not only the resistance to mixing of the local concentration contrasts but also the deviation of the mean concentration from the Gaussian distribution. The rest of the section is devoted to describe the computation of γ and the mixing states.

2.1. Model and Numerical Methods

[13] The model and numerical methods to simulate flow and transport are classical. Our implementation is essentially that of *Beaudoin et al.* [2007] and *de Dreuzy et al.* [2007]. We summarize it below for the sake of completeness.

[14] The permeability field is modeled by a 2-D lognormal field with an isotropic gaussian correlation function:

$$\langle Y'(\mathbf{x})Y'(\mathbf{x}')\rangle = \sigma_Y^2 \exp\left(-\left(\frac{|\mathbf{x}-\mathbf{x}'|}{\lambda}\right)^2\right), \tag{11}$$

where $Y'(\mathbf{x}) = Y(\mathbf{x}) - \langle Y\rangle$ and $Y(\mathbf{x}) = \ln(K(\mathbf{x}))$, $\langle\ \rangle$ stands for spatial (ensemble) average, σ_Y^2 is the lognormal permeability variance and λ is the correlation length. The computational domain is a rectangle of dimensions L_1 and L_2 in the two spatial dimensions x_1 and x_2 counted in terms of correlation length (L_1/λ, L_2/λ).

[15] Periodic boundary conditions are imposed both on the permeability field and on the flow equation at the horizontal domain boundaries to ensure that the velocity statistics are not biased by the boundaries, in contrast to the no-flow boundary conditions case [*Englert et al.*, 2006; *Salandin and Fiorotto*, 1998]. Typical examples of permeability fields are displayed on the top line of Figure 2. Even if the correlation pattern remains the same from right ($\sigma_Y^2 = 1$) to left ($\sigma_Y^2 = 9$), the amplitude of variation increases steeply from 3 to 8 orders of magnitude. The second line of Figure 2 also shows the enhancement of flow channeling with higher flow contrasts and more continuous flow channels [*Le Goc et al.*, 2009].

[16] Solute is transported by advection and diffusion. the ratio of advection to diffusion is described by the peclet number:

$$Pe = (\lambda \cdot \overline{u})/d_0, \tag{12}$$

where $\overline{u}$ is the mean velocity. Injection is instantaneous on the full width of the domain L_2 orthogonally to the main flow direction along x_1. Injection is shifted downstream from the domain inlet by a distance of 10 λ from the domain inlet to avoid boundary effects. Injected concentrations are either proportional to flow or uniform.

[17] The flow equation is solved numerically using finite differences with square grid cells ($dx_1 = dx_2 = l_m$). Solute transport is simulated using a classical random walk method. The aspect ratio of the system L_1/L_2 ranges from 1 to 4. As we are interested both in the preasymptotic and in the asymptotic regimes, we have used a large range of system sizes L_1/λ, L_2/λ between 200 and 800. The injection window has a width of at least 100 λ. The number of grid cells per correlation length λ/l_m is not smaller than 10 [*Ababou et al.*, 1989]. An initial convergence analysis shows that 5000 particles per simulation corresponding to around 10 particles per correlation length and 100 Monte-Carlo simulations are sufficient to get accurate estimates of the mixing states. Finally, we consider wide ranges both for heterogeneity ($0.25 \leq \sigma_Y^2 \leq 9$) and Peclet numbers ($50 \leq Pe \leq 10^3$).

[18] In the following, time t is rescaled by the advection time scale $\tau_u = \lambda/\overline{u}$, which defines the dimensionless time $t' = t/\tau_u$. For simplicity of notation in the following, we drop the prime.

2.2. Computation of Mixing States

[19] As defined by equation (3), the overall mixing state $M(t)$ is equal to the spatial integral of the concentration squared. Concentrations can be approximated by the average number of particles over a fixed grid cell scale. However, the average distance between particles increases and concentrations become increasingly noisy as time proceeds. *Le Borgne et al.* [2011] found that a much more accurate method to compute $M(t)$ is based on the cumulative distribution of particle pair separation distance, $P(r, t)$ [*Fiori and Dagan*, 2000; *Tonina and Bellin*, 2008]. Using this distribution, the concentration second moment becomes [*Grassberger and Procaccia*, 1983]:

$$\lim_{r \to 0} \frac{P(r,t)}{\pi r^2} = \int_\Omega c(\rho,t)^2 d\rho = M(t). \tag{13}$$

[20] In practice, r should be chosen smaller than the mixing scale $\varepsilon(t)$, defined as the smallest scale over which c can be considered uniform, but still larger than the smallest distance between particles. In fact, the normalized pair particle separation distance (13) is independent on the scale r, for $r < \varepsilon(t)$.

[21] The dispersive mixing state $M_1(t)$ is the integral over the domain of the average concentration $\overline{c}$ squared as stated by equation (6). We define $\overline{c}$ as the average of the concentration over transects orthogonal to the mean flow direction:

$$\overline{c}(x_1,t) = \frac{\int_0^{L_2} c(x_1,x_2,t)\, dx_2}{L_2}. \tag{14}$$

[22] $M_1(t)$ could be computed by first determining $\overline{c}$ and then integrating its square over the domain extension. However, for the sake of consistency and accuracy, we adopt the same methodology as for $M(t)$ but in the x_1 direction. $M_1(t)$ is computed from the cumulative distribution of the pair particle separation distance along the x_1 coordinate $P_1(x_1, t)$. For small enough distances, the x_1 distribution of particles is homogeneous and $P_1(x_1, t)$ is related to the second moment of average concentrations by:

$$\lim_{l_1 \to 0} \frac{P_1(l_1,t)}{2l_1} = \int_0^{L_1} \overline{c}^2(x_1,t) dx_1 = M_1(t). \tag{15}$$

[23] As for $M(t)$, $M_1(t)$ is equal to the pair particle density when the distance l_1 is smaller than some characteristic scale of the order of the mixing scale.

[24] As discussed in the introduction, the potential macrodispersive mixing state $M_D(t)$ is the mixing state corresponding to a Gaussian plume that has the same longitudinal dispersion σ_L as the real plume. It can be straightforwardly obtained from equation (9).

[25] Finally, $M_2(t)$ and $\gamma(t)$ are not computed from the concentration field but deduced from the above mixing states by using equation (8) for γ and the decomposition given by equation (5) for M_2:

$$M_2(t) = M(t) - M_1(t). \tag{16}$$

2.3. Difference Between Spreading and Gaussian Mixing States M_1 and M_D

[26] As stated in the introduction, if the average concentration $\overline{c}(x_1)$ was indeed Gaussian, then $M_D(t)$ would be equal to $M_1(t)$ [*Kapoor and Gelhar*, 1994b; *Kapoor and Kitanidis*, 1998]. While this is a good approximation for weak heterogeneity or late times, it is in general not true for strong heterogeneity and at early times. Numerical results obtained for $\sigma_Y^2 = 9$ show that, around the advection time ($t = 1$), the distribution is highly skewed and biased to the smaller values (Figure 1, black curves scaled on the left axis). From the advection time ($t = 1$) to ten times the advection time ($t = 10$) (Figure 1), the skewness is divided by a factor of 4 and asymptotically the mean concentration profile becomes Gaussian even for highly heterogeneous media.

[27] The deviation of the mean concentration from a Gaussian distribution is larger for uniform injection conditions

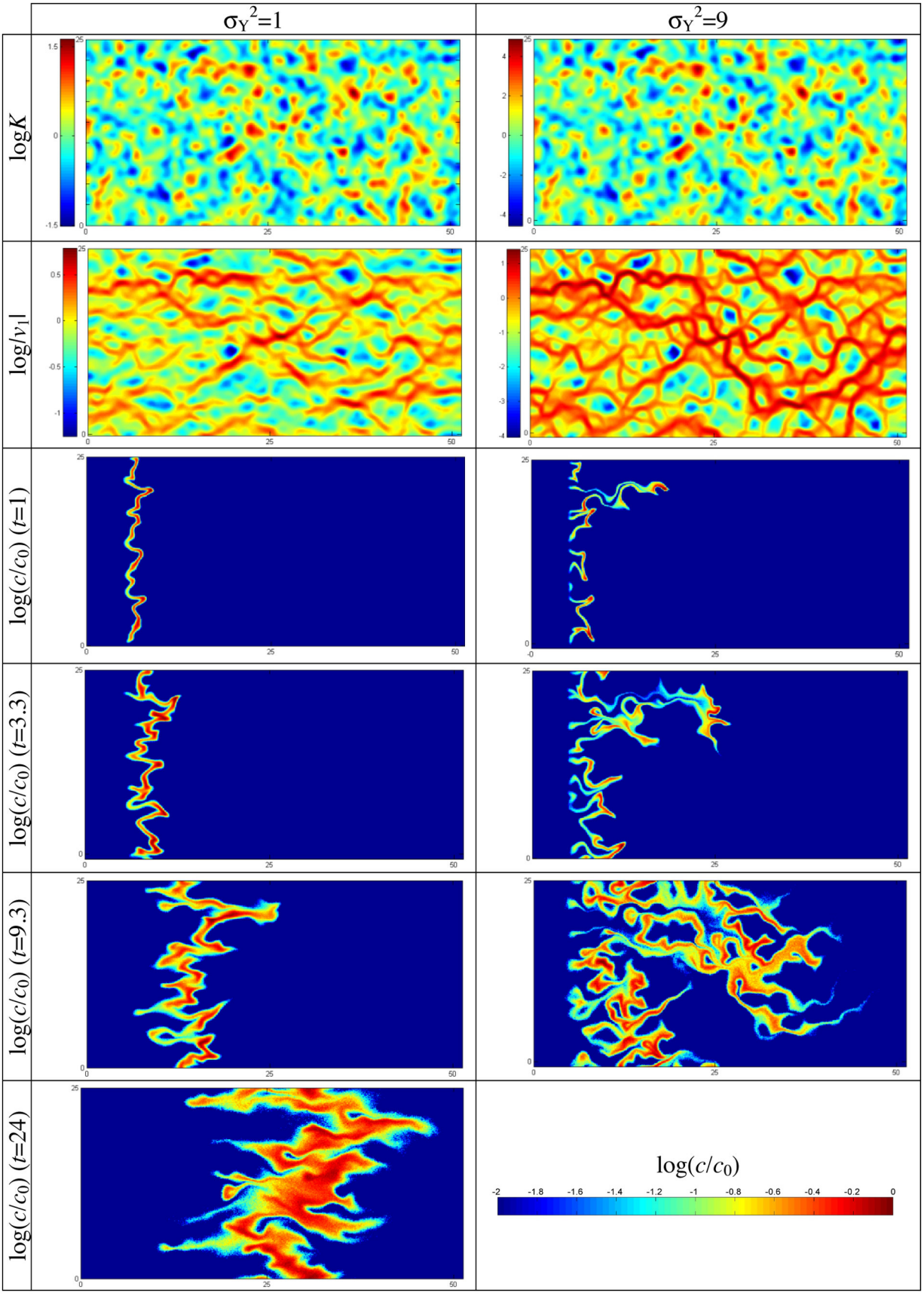
σY²=1
σY²=9
log K
log|v1|
log(c/c0) (t=1)
log(c/c0) (t=3.3)
log(c/c0) (t=9.3)
log(c/c0) (t=24)
log(c/c0)
-2 -1.8 -1.6 -1.4 -1.2 -1 -0.8 -0.6 -0.4 -0.2 0

Figure 2

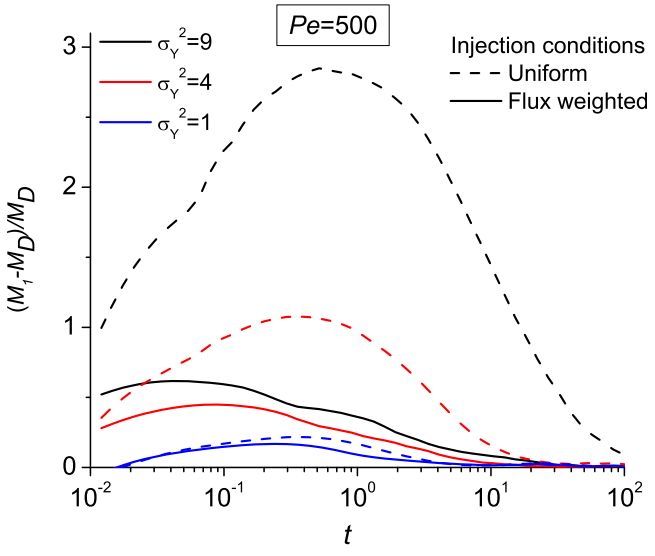

Figure 3. $(M_1 - M_D)/M_D$ for evolving levels of heterogeneity at Peclet number $Pe = 500$ for flux-weighted and uniform injection conditions at evolving levels of heterogeneity.

than for flux-weighted injection conditions (Figure 1, dashed lines) because a large portion of the injected mass lags behind at low K areas. In fact, the early time average concentration $\overline{c}$ is determined by the velocity distribution rather than by diffusion. For example, for a stratified medium with the same velocity point-distribution $p(u)$ as the heterogeneous flow field under consideration and uniform or flux-weighted injection conditions, the plume shape directly derives from the velocity distribution and is $p(u)$ and $u \cdot p(u)/\overline{u}$, respectively. For mildly to highly heterogeneous permeability fields ($\sigma_Y^2 \geq 1$), the velocity distribution $p(u)$ is close to a lognormal distribution [*Salandin and Fiorotto*, 1998], for which $p(u)$ is more skewed and biased to the smaller values than $u \cdot p(u)/\overline{u}$.

[28] In summary, M_1 deviates from M_D in the preasymptotic regime. We characterize this deviation by the ratio $(M_1 - M_D)/M_D$ (Figure 3), which is positive. The ratio first increases with time, reaching a maximum at a time around the advection time in the uniform injection case and much earlier in the flux-weighted injection case. Differences vanish only after some advection times. The deviation from the Gaussian behavior is enhanced by heterogeneity and is already non-negligible at mild levels of heterogeneity ($\sigma_Y^2 = 1$) (Figure 3, blue curves). M_1 cannot thus be identified to M_D on a broad interval of times around the advection time scale for mildly to highly heterogeneous media ($\sigma_Y^2 \geq 1$). The relative difference between M_1 and M_D is enhanced both by the heterogeneity and by the uniform injection conditions.

2.4. Overall Variations of the Deviation From the Potential Macrodispersive Mixing $\gamma(t)$

[29] We evaluate numerically the relative deviation γ of the actual mixing state from the potential macrodispersive

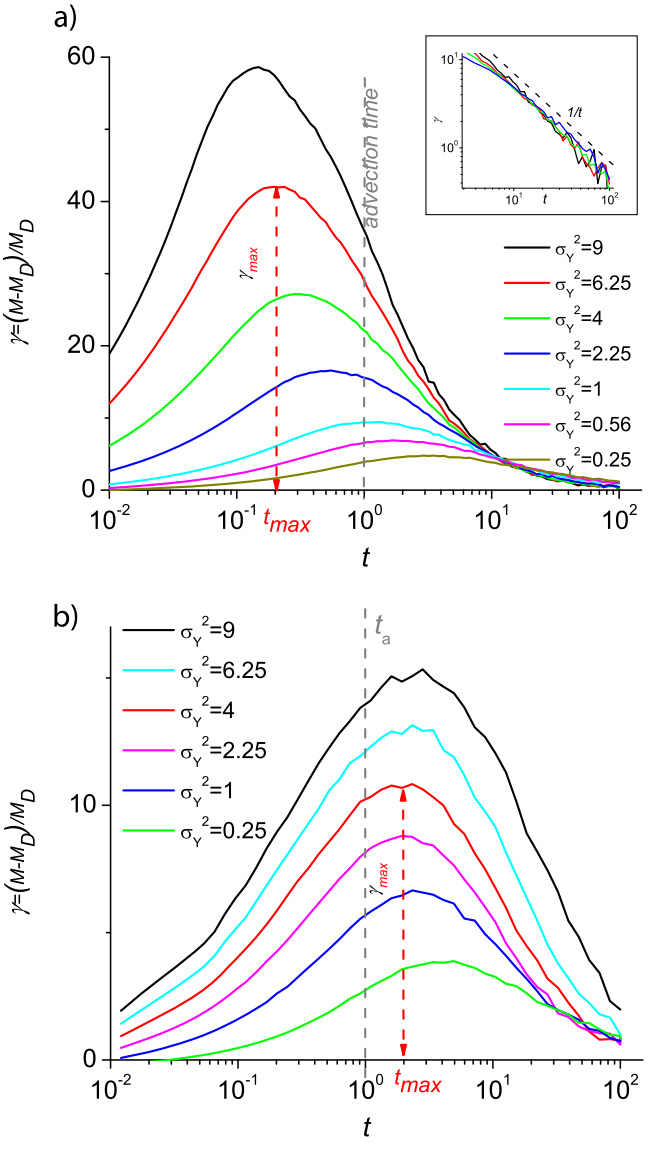

Figure 4. $\gamma = (M - M_D)/M_D$ for evolving levels of heterogeneity at Peclet number $Pe = 500$ for flux-weighted (a) and uniform (b) injection conditions. Insert of (a) shows the late time behavior of γ compared to the $1/t$ tendency (dashed line).

(Gaussian) mixing state. It depends on a number of factors including the heterogeneity variance (σ_Y^2), Peclet number (Pe) and the solute injection conditions (uniform or flux weighted).

[30] Figure 4 displays the typical variations of γ for a Peclet number of 500. γ has a roughly symmetrical bell-shaped behavior in logarithmic-linear coordinates expressing a sharp rise and a slow decrease for all simulation conditions. Its maximum γ_{max} occurs around the advection

Figure 2. From top to bottom: log K field, log$|v_1|$ field and log(c/c_0) at four evolving times on the left ($t = 1$, 3.3, 9.3 and 24) for $\sigma_Y^2 = 1$ and at these three first times on the right for $\sigma_Y^2 = 9$. Initial concentrations are flux weighted, Peclet number is 100 and system sizes are $L_1/\lambda = 2L_2/\lambda = 51.2$, i.e., one fourth to one tenth of the characteristic sizes used in this study. Both fields have the same correlation structure but different permeability variability. If channels are located in the same areas, they are more pronounced in the higher heterogeneity case on the right.

time scale. As the sharp rise occurs earlier than the advection time, it is likely that it comes from the heterogeneity of the velocity field. Indeed, the ensemble dispersion coefficient, whose behavior is dominated by advective heterogeneity, increases sharply in this time range [*Dentz et al.*, 2000]. The potential macrodispersive mixing state $M_D(t)$ decreases accordingly, see equation (9).

[31] The heterogeneity in the velocity field generates long filaments enhancing plume spreading as displayed by the early-time concentration fields of the third and fourth lines from top of Figure 2. In the absence of diffusion, γ increases without limits. Diffusion limits the increase of γ by smoothing out the filament structure created by the heterogeneous velocity field (5th line from top of Figure 2). Eventually at large times, γ tends asymptotically to zero as $1/t$ (Figure 4, insert) and the plume becomes nearly well mixed within the full spreading area (bottom line of Figure 2).

[32] In the preasymptotic regime, γ increases with the heterogeneity variance σ_Y^2 as heterogeneity enhances the velocity field correlation (Figure 2, second line from top) [*Le Borgne et al.*, 2007]. It is traduced by the enhancement of the filaments in the concentration fields from the left ($\sigma_Y^2 = 1$) to the right ($\sigma_Y^2 = 9$) of Figure 2. For $\sigma_Y^2 \geq 1$, γ is also strongly influenced by the injection conditions (Figure 4a versus Figure 4b). Initially, γ is positive for flux-weighted injection conditions but null for uniform injection conditions. This initial difference propagates at least over the advection-dominated regime and is progressively dampened by diffusion.

[33] Finally we compare $\gamma(t) = (M(t) - M_D(t))/M_D(t)$ as given by Figure 4 with the relative deviation $(M_1(t) - M_D(t))/M_D(t)$ studied in section 2.3 and given by Figure 3. In the uniform injection case, $(M_1(t) - M_D(t))/M_D(t)$ is of the order of 10% to 20% of $\gamma(t)$, so that $M_1(t)$ cannot be identified to the potential macrodispersive mixing state $M_D(t)$. In the flux-weighted injection case however, $(M_1(t) - M_D(t))/M_D(t)$ is of the order of 1% to 2% of $\gamma(t)$. It does not mean that the average concentration does no longer depart from a Gaussian distribution as previously stated. It just means that the initial concentration heterogeneity and the advective heterogeneities have a much stronger effect on the overall mixing state than the non-Gaussianity of the mean concentration. In the flux-weighted injection case, we will approximate $M_1(t)$ by $M_D(t)$ in an attempt to derive $\gamma(t)$ from macrodispersion.

3. Analytical Derivation of $\gamma(t)$ for Flux Weighted Injection

[34] In this section, we approximate $M_1(t)$ by $M_D(t)$ and consequently $M_2(t)$ by $\gamma(t) \cdot M_D(t)$. As the local mixing state $M_2(t)$ is also the spatially integrated concentration variance $\|\sigma_c^2\|$, we attempt to derive $\gamma(t)$ from the knowledge acquired on concentration variance [*Andricevic*, 1998; *Caroni and Fiorotto*, 2005; *Fiori and Dagan*, 2000; *Fiorotto and Caroni*, 2002; *Kapoor and Gelhar*, 1994a, 1994b; *Kapoor and Kitanidis*, 1998; *Tonina and Bellin*, 2008; *Vanderborght*, 2001]. It should be noted however that the problem handled here still differs from previous ones by the magnitude of the permeability variability considered. While all previous studies on concentration variance have dealt with low to mild heterogeneity permeability fields ($\sigma_Y^2 \leq 1$), we focus here on mild to high heterogeneity fields ($\sigma_Y^2 \geq 1$). The difference is not minor as both cases may lead to fundamentally different behaviors. For example, spreading by permeability heterogeneity is strongly enhanced by heterogeneity when $\sigma_Y^2 \geq 1$ [*de Dreuzy et al.*, 2007; *Jankovic et al.*, 2003].

[35] Using the Eulerian approach, *Kapoor and Gelhar* [1994a] derive the equation for the evolution of concentration variance:

$$\frac{d}{dt}\|\sigma_c^2\| = \sum_{i=1}^{2} 2D_{ii}\left\|\left(\frac{\partial \overline{c}}{\partial x_i}\right)^2\right\| - 2d\left\|\left(\frac{\partial c'}{\partial x_i}\right)^2\right\|, \qquad (17)$$

in which D denotes the diagonal macrodispersion tensor, and $\|\cdot\|$ stand for integration over the flow domain, Ω. The off-diagonal dispersion terms are supposed to be zero because of the isotropic nature of the permeability field and because the main flow direction is aligned with the x_1 coordinate. Equation (17) expresses that concentration variance $\|\sigma_c^2\|$ is generated by spreading (effective dispersion) and destroyed by diffusion. Without mass flux through the domain boundaries and for pulse-like injection conditions, the first term on the right side of equation (17) is directly linked to $M_1'(t)$, where we use the shorthand notation $f'(t) = df(t)/dt$ for the time derivative (Appendix A of *Le Borgne et al.* [2010]):

$$\sum_{i=1}^{2} 2D_{ii}\left\|\left(\frac{\partial \overline{c}}{\partial x_i}\right)^2\right\| = -\frac{d}{dt}\left(\int_{\Omega} d^d x\, \overline{c}^2\right) = -M_1'(t). \qquad (18)$$

[36] The second term has been classically approximated by the interaction by exchange with the mean closure approximation (IEM closure) [*Kapoor and Gelhar*, 1994a; *Tennekes and Lumley*, 1972; *Villermaux and Devillon*, 1972]

$$\left\|\left(\frac{\partial c'}{\partial x_i}\right)^2\right\| = \frac{\|\sigma_c^2\|}{\Delta^2}, \qquad (19)$$

where Δ is the concentration microscale characterizing the typical spatial scale of concentration perturbation c' variations. Replacing $\|\sigma_c^2\|$ by $M_2(t)$, using equations (18) and (19) and approximating $M_1(t)$ by $M_D(t)$, equation (17) can be written as

$$M_2'(t) + \frac{2d}{\Delta^2} M_2(t) = -M_D'(t). \qquad (20)$$

[37] The only difficulty for solving equation (20) lies in the evaluation of Δ.

[38] Δ has first been assumed to be constant [*Kapoor and Gelhar*, 1994a]. It has been analytically expressed as the result of the balance between compression induced by advection and expansion due to diffusion [*Tennekes and Lumley*, 1972]. Evaluated later numerically from the concentration perturbation c' and its gradient, Δ has been found to first increase before reaching an asymptotic value at times larger than the diffusion time scale [*Kapoor and Kitanidis*, 1998]. While this method gives valuable insight into the evolution of the concentration microscale Δ, it does not provide an independent way to obtain $\|\sigma_c^2\|$.

[39] Here we propose replacing the concentration microscale Δ by the mixing scale ε defined as the largest scale

over which the concentration can be considered locally uniform [*Le Borgne et al.*, 2011]. For a homogeneous media ε grows diffusively and it is equal to the diffusion scale $\sqrt{2Dt}$. For heterogeneous media it has been found to scale subdiffusively with time due to the competition between local shear and diffusion. Note that, unlike Δ, which is defined by equation (19), ε can be determined independently of the concentration variance. We thus determine $M_2(t)$ by solving the following equation:

$$M_2'(t) + \frac{2d}{(a\,\varepsilon(t))^2} M_2(t) = -M_D'(t), \tag{21}$$

which is equivalent to equation (20) where the concentration microscale Δ has been replaced by $a\,\varepsilon(t)$. The prefactor a expresses the possible difference between Δ and ε by a constant multiplicative factor that does not alter the scaling evolution of ε. We have solved equation (21) numerically with $M_D(t)$ given by equation (9), $\sigma_L(t)$ and $\varepsilon(t)$ obtained from the numerical simulations. Without any additional information, the prefactor a had to be optimized to minimize the difference of the values of γ derived from equation (21) and obtained numerically. Figure 5 shows the good agreement between the values of γ obtained directly from the simulations (solid lines) and obtained from the numerical integration of (21) (dashed lines). Values of the prefactor a remain close to 1 in the interval [0.72, 0.8].

[40] The derivation of M_2 from equation (21) depends both on the scaling of the mixing scale ε and on the prefactor a. To assess the sensitivity of the equation to the scaling of the mixing scale ε, we have analyzed the effect of a small alteration of the scaling of ε by multiplying ε by $t^{0.05}$ while keeping the same integration method for equation (21) (Figure 5). Despite the optimization of the prefactor a, the dashed-dotted lines significantly depart from the numerical results (solid lines) demonstrating the high sensitivity of γ to the scaling of the mixing scale ε.

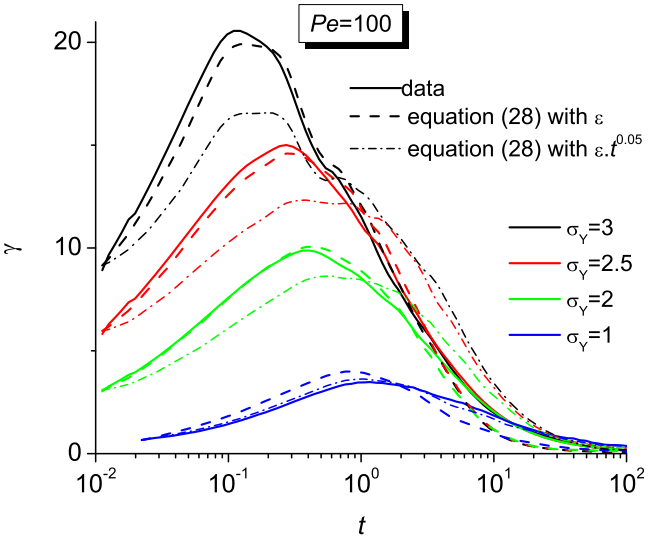

Figure 5. Numerical results for the relative deviation from the Potential macrodispersive mixing regime (full lines) compared to the result of the integration of equation (21) with the externally provided ε and the fitted value of the prefactor a (dashed lines) at Peclet of 100. Dashed-dotted lines come from the integration of equation (21) with an altered scaling of ε by $t^{0.05}$.

[41] The fact that small deviations from the mixing scale cause large deviations in γ reinforces both the concentration variance equation (18) and the mixing scale concepts, which were derived independently. That is, the approximations made by *Kapoor and Gelhar* [1994a] in deriving equation (17) are appropriate and the concentration microscale must be proportional to the mixing scale. This result also supports the proposed mixing concept in that the mixing state is solely determined by the extension of the plume (spreading scale) and the support scale of the concentration (mixing scale). However, given the current state of knowledge, the previous analysis has some weak points. First, the determination of the mixing scale requires the knowledge of the concentration field. The information available on the mixing scale is yet insufficient to lead to a general independent characterization especially at early times. Second, the derivation of the overall mixing state from the mixing scale is highly sensitive to the time scaling of the mixing scale. Estimate of the mixing scale must thus be highly accurate. Third, the prefactor a has not yet been determined independently and must be fitted. Finally, this approach is not general and relies on the possibility to approximate $M_1(t)$ by $M_D(t)$ which can be reasonably attempted in the flux-weighted injection case but not in the uniform injection case. While one may hope that these limitations will be overcome, we seek for a simple alternative characterization of $\gamma(t)$ in section 4.

4. Toward a Generic Characterization of γ

[42] Whatever the Peclet number, permeability heterogeneity and injection conditions, γ always has a maximum. The value of the maximum is noted γ_{max} and the time at which it occurs t_{max}. γ also always display a bell-shaped curve with a sharp rise and a slow decrease (Figure 4). We show in this section that γ_{max} and t_{max} are simple functions of the model parameters and that the bell-shaped time evolution of $\gamma(t)$ is highly generic.

4.1. Maximum of the Relative Deviation From the Potential Macrodispersive Mixing State

[43] Figure 6 displays the evolution of $\gamma_{max}/\sqrt{Pe}$ as a function of σ_Y^2 for different Peclet numbers. It first shows that γ_{max} scales with $\sqrt{Pe}$. This tendency is at least qualitatively logical as less diffusion (higher values of Pe) induces higher deviations to the potential macrodispersive mixing state. The fact that the scaling factor is precisely $\sqrt{Pe}$ is also natural, because the diffusion scale grows with $\sqrt{d_0 t}$.

[44] As stated in 2.4, deviations from potential macrodispersive mixing are enhanced by both permeability heterogeneity and flux-weighted injection conditions. Consistently, γ_{max} increases with σ_Y^2 and flux-weighted injection conditions enhance γ_{max} by a factor of 1.6 at $\sigma_Y^2 = 2.25$ and by a factor of 2.5 at $\sigma_Y^2 = 9$. For flux-weighted injection conditions and $\sigma_Y^2 > 1$, γ_{max} scales approximately as $\sigma_Y^2/4$ (gray line on Figure 6). For $\sigma_Y^2 < 1$, the difference between flux-weighted and uniform injection conditions vanishes (Figure 6, insert). More precisely, the difference becomes indistinguishable for $\sigma_Y^2 \approx 0.4$. At smaller values of σ_Y^2, γ_{max} drops quickly to

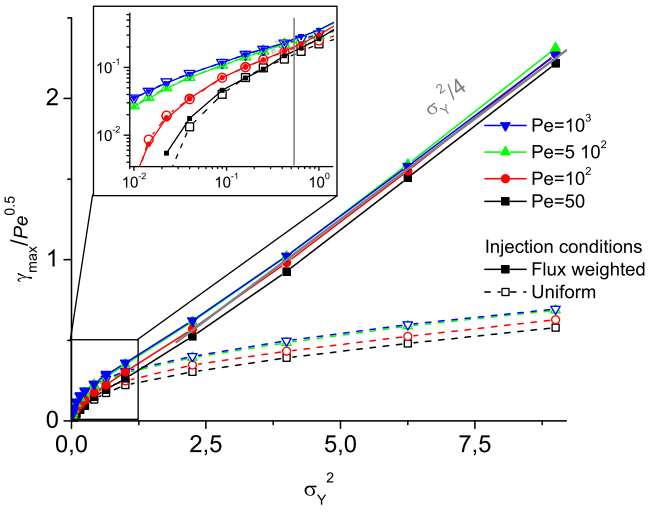

Figure 6. Maximum of the relative deviation from the potential macrodispersive mixing regime γ_{max} normalized by $\sqrt{Pe}$ as a function of σ_Y^2 for flux-weighted and uniform injection conditions. Insert shows the small heterogeneity behavior of $\gamma_{max}/\sqrt{Pe}$.

zero first linearly and then even quicker. In fact, γ should vanish at low heterogeneity where concentrations are solely determined by diffusion.

[45] Similarly, the time t_{max} does not depend on the injection conditions for low level of heterogeneities ($\sigma_Y^2 < 0.1$). At higher levels of heterogeneity however, t_{max} stabilized between 1.5 and 2.5 advection time scales for uniform injection while it decreases approximately as $1/\sigma_Y^2$ for flux-weighted injection (Figure 7).

[46] At low levels of heterogeneity, the behaviors of γ_{max} and t_{max} are qualitatively similar to those found for the concentration variance by numerical and perturbation methods [*Tonina and Bellin*, 2008]: "a larger formation heterogeneity results in an earlier and higher peak of the concentration variance". While this conclusion holds for higher levels of heterogeneity and flux-weighted injection conditions, it does not apply to uniform injection conditions where t_{max} becomes independent of the heterogeneity while γ_{max} still increases.

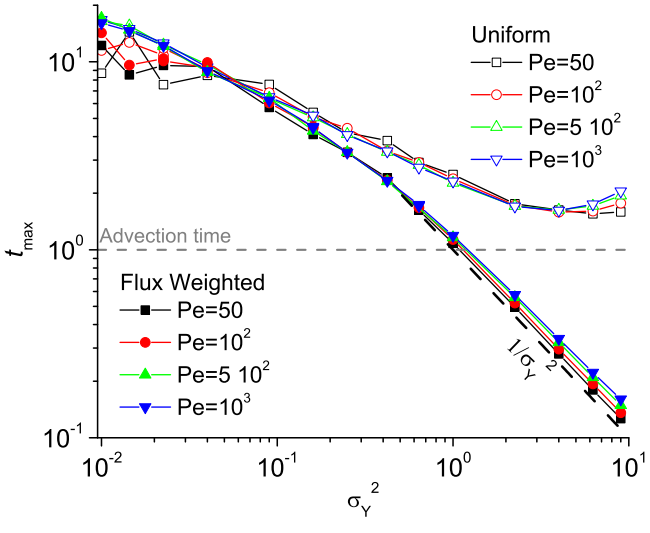

Figure 7. Time t_{max} at which the maximum of the relative deviation from the potential macrodispersive mixing regime occurs.

[47] The surprising result is that t_{max} is almost insensitive to variations of the Peclet number *Pe*. One might expect a marked dependence of t_{max} on diffusion. The weak influence of variations of *Pe* indicates that the variations of γ are controlled by advection rather than diffusion. The proximity of t_{max} to the advection time scale corroborates this conclusion, which is qualitatively explained by Figure 2. Internal disorder (i.e., incomplete mixing within the plume) is initially controlled by the variability of velocity (see graphs for $t = 1$ and 3.3 in Figure 2). A very significant destruction of concentration variance occurs because of the convergence of high velocity paths around low-velocity islands. While the actual mixing caused by convergence is sensitive to *Pe* (so that γ_{max} should be proportional to $\sqrt{Pe}$), the topology of the flow paths (and, therefore, t_{max}) is not. In summary, while the magnitude of the deviation from dispersive mixing is highly dependent on local diffusion, the time at which the deviation is maximum depends instead on the topology of the velocity field.

4.2. Scaling Form For γ

[48] Beyond the characteristic of its maximum (γ_{max}, t_{max}), we show that the time evolution of $\gamma(t)$ displays a well defined scaling behavior. Figure 8 illustrates $\gamma(t)/\gamma_{max}$ as a function of t/t_{max} for different initial conditions and heterogeneity variances. It has a bell-shaped form as discussed above. Using this scaling, the displayed behavior is almost independent from the injection mode and heterogeneity variance suggesting the scaling form

$$\gamma(t) = \gamma_{max} f\left(\frac{t}{t_{max}}\right) \tag{22}$$

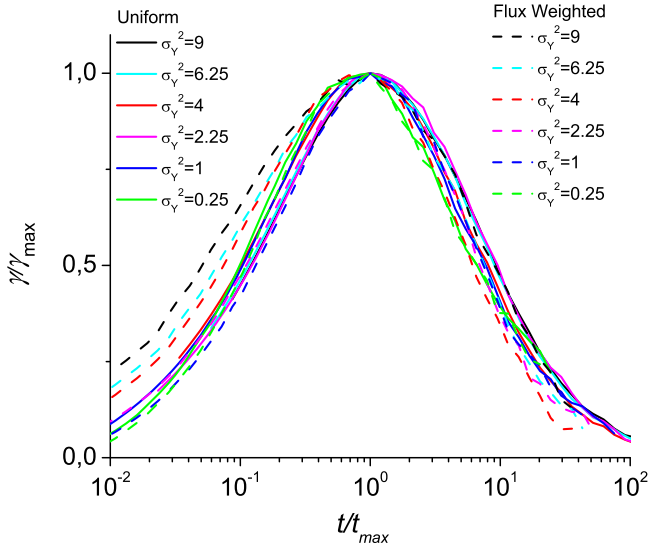

Figure 8. Relative deviation from the potential macrodispersive mixing regime γ normalized by its maximum γ_{max} as a function of the time t normalized by t_{max} for flux-weighted and uniform injection conditions at evolving levels of heterogeneity.

for $\gamma(t)$. The largest deviations from this scaling occur at small times for large heterogeneity variance and uniform injection conditions. Apart from these cases, the variability of γ/γ_{max} around the scaling form (22) is less than 10%, which is very small compared to the range of different heterogeneity, diffusion and injection conditions involved.

[49] A byproduct of this simple scaling is that, for flux-weighted initial conditions, the dependence of γ on the model parameters can be simply expressed from the dependences established for γ_{max} and t_{max} in the previous section,

$$\gamma(t) \approx \frac{\sqrt{Pe}\,\sigma_Y^2}{4} f(\sigma_Y^2\, t). \tag{23}$$

[50] Asymptotically, $\gamma(t) \sim \sqrt{Pe}/(4\,t)$. The dependence on the model parameters is more complex for the uniform injection case. This generic scaling behavior is surprising. It means that γ/γ_{max} does neither depend on the Peclet number nor on the level of heterogeneity σ_Y^2. The independence of this scaling behavior has several consequences. First, $f(t)$ might be approximated analytically with perturbative methods for low heterogeneity and then extended to a broad range of different heterogeneity levels, Peclet values and injection conditions. Second, we can derive from the generic scaling form f some general conclusions on mixing. As $\gamma(t)$ expresses the transition between local mixing by diffusion at very early time to global mixing by macrodispersion at late times, the transition between these two extreme regimes always extend over the same range of temporal scales. For example the time range over which γ/γ_{max} is larger than one fourth of its maximum extends over 2.5 orders of magnitude. It is independent of the rate of advection to diffusion, of the heterogeneity and of the injection conditions. It can be taken as a rough estimate of the time range of the transition between the local mixing by diffusion regime and the global mixing by macrodispersion regime.

[51] The same type of fast rise and slow decrease of γ can also be observed for transport in viscous flow through a channel, which at large times can be fully described by Taylor dispersion (Figure 9). γ has been computed for uniform injection conditions from the analytical solutions for M_2 and M_D derived in the work of *Bolster et al.* [2011] using a volume-averaging approach. At sufficiently low values of the Peclet number ($Pe < 50$), γ_{max} strongly increases with the Peclet number while the time t_{max}, at which the maximum is reached is constant. The dependence of γ/γ_{max} as a function of t/t_{max} is also independent of the Peclet number and increases initially linearly with time and at late times like the inverse of time. These results are qualitatively similar to what has been obtained here for correlated heterogeneous porous media in the sense that t_{max} is constant, that γ_{max} increases with the Peclet number and that the generic scaling displays the same early and late time evolutions. Quantitatively however, the rate of increase of γ_{max} with Pe is much higher for stratified k fields than for the correlated fields analyzed here, while the values of γ_{max} are much smaller. The generic scaling of equation (22) with a function f increasing first linearly with time and decreasing eventually as the inverse of time might thus be a characteristic generic to a broader range of flow fields.

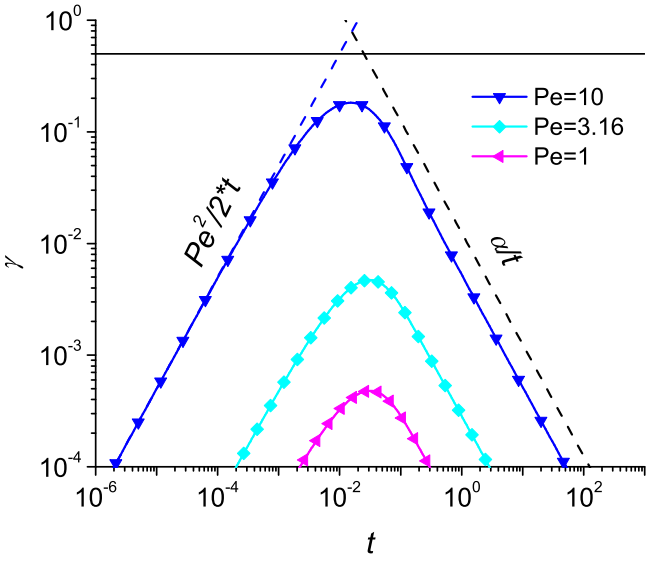

Figure 9. Relative deviation from the potential macrodispersive mixing regime γ for Taylor dispersion.

5. Conclusions

[52] Mixing results from the interplay between the local-scale concentration variability (internal plume disorder) and the global scale dispersion (rate of spreading of the plume). Classical characterization of mixing has relied on the decomposition of the concentration in a mean concentration and a deviation about it. To be tractable analytically, this decomposition generally requires the mean concentration to be Gaussian. This is indeed the case for low heterogeneity or late times (times larger than the characteristic diffusion time). However, in all other cases, the mean concentration can be significantly non Gaussian.

[53] Mixing is quantified by the overall mixing state $M(t)$ defined as the integral of the concentration squared. Here, we have decomposed this mixing state as the sum of a potential macrodispersive mixing state $M_D(t)$ plus a departure term, $\gamma(t) \cdot M_D(t)$. We define the potential macrodispersive mixing state $M_D(t)$ as the integrated squared concentration of the Gaussian plume that has the same longitudinal dispersion as the real plume (9). The deviation function $\gamma(t)$ is the difference of the overall mixing state $M(t)$ and the potential macrodispersive mixing state, $M_D(t)$, normalized by the latter. This definition facilitates taking full advantage of prior knowledge on dispersion for characterizing mixing, even when the mean solute concentration field is highly non Gaussian.

[54] We determine the relative deviation to the potential macrodispersive mixing state γ numerically on classical log normally Gaussian correlated permeability fields with extended uniform injection and flux-weighted boundary conditions. γ increases sharply at first because of the velocity variability and decreases slowly to zero because of the homogenization effect of diffusion. γ reaches its maximum γ_{max} at time t_{max}, which ranges from one 10th to ten advection times.

[55] An analytical derivation is possible in the flux-weighted injection case, where mean concentration is indeed Gaussian. We can adopt the equation for the evolution of concentration variance (21) to show that γ can be derived

from the spreading scale of the plume and the local mixing scale, defined as the maximum scale over which solute concentrations remain uniform. Departure from Gaussianity of the mean concentration precludes this approach for uniform injection conditions.

[56] We thus propose an alternative characterization of γ based on γ_{max}, t_{max} and a generic function f (equation (22)). Heterogeneity globally enhances the deviation from the dispersive mixing through the increase of γ_{max} with σ_Y^2 but reduces the time t_{max} to reach it. Diffusion reduces the deviation from the dispersive mixing regime but surprisingly does not alter the characteristic time t_{max}, which is sensitive to the topology of the velocity field. While γ_{max} and t_{max} are specific, the general evolution of γ does not depend on diffusion, heterogeneity, or injection conditions. γ is thus simply characterized by its maximum characteristics γ_{max} and t_{max} and a generic temporally evolving function f. The shape of the generic function f might even not depend on the particularities of the flow fields as the same generic shape also prevails for Taylor dispersion. This generic characterization of mixing can offer new ways to set up transport equations that honor not only advection and spreading (dispersion), but also mixing.

[57] **Acknowledgments.** The European Union is acknowledged for its funding through the Marie-Curie fellowship PIEF-GA-2009-251710 and the MUSTANG project (UE-7thFP-ENERGY 227,286). Additional funding was provided by the French National Research Agency ANR through the MICAS project for the development of parallel simulation methods (ANR-07-CIS7-004) and by the Fundación Ciudad de la Energía (CIUDEN).

References

Ababou, R., et al. (1989), Numerical simulation of three-dimensional saturated flow in randomly heterogeneous porous media, *Transp. Porous Media*, *4*(6), 549–565.

Andricevic, R. (1998), Effects of local dispersion and sampling volume on the evolution of concentration fluctuations in aquifers, *Water Resour. Res.*, *34*(5), 1115–1129.

Beaudoin, A., et al. (2007), An efficient parallel tracker for advection-diffusion simulations in heterogeneous porous media, *Europar*, Springer, Berlin.

Bolster, D., et al. (2011), Mixing in confined stratified aquifers, *J. Contam. Hydrol.*, *120–121*, 198–212.

Caroni, E., and V. Fiorotto (2005), Analysis of concentration as sampled in natural aquifers, *Transp. Porous Media*, *59*(1), 19–45.

Chiogna, G., O. A. Cirpka, P. Grathwohl, and M. Rolle (2011), Transverse mixing of conservative and reactive tracers in porous media: Quantification through the concepts of flux-related and critical dilution indices, *Water Resour. Res.*, *47*, W02505, doi:10.1029/2010WR009608.

Cirpka, O. A., and P. K. Kitanidis (2000), Characterization of mixing and dilution in heterogeneous aquifers by means of local temporal moments, *Water Resour. Res.*, *36*(5), 1221–1236.

Dagan, G. (1989), *Flow and Transport in Porous Formations*, 465 pp., Springer, New York.

de Dreuzy, J.-R., et al. (2007), Asymptotic dispersion in 2D heterogeneous porous media determined by parallel numerical simulations *Water Resour. Res.*, *43*, W10439, 10.1029/2006WR005394.

Dentz, M., H. Kinzelbach, S. Attinger, and W. Kinzelbach (2000), Temporal behavior of a solute cloud in a heterogeneous porous medium, 2, Spatially extended injection, *Water Resour. Res.*, *36*(12), 3605–3614, doi:10.1029/2000WR900211.

de Simoni, M., J. Carrera, X. Sanchez-Vila, and A. Guadagnini (2005), A procedure for the solution of multicomponent reactive transport problems, *Water Resour. Res.*, *41*, W11410, doi:10.1029/2005WR004056.

Englert, A., J. Vanderborght, and H. Vereecken (2006), Prediction of velocity statistics in three-dimensional multi-Gaussian hydraulic conductivity fields, *Water Resour. Res.*, *42*, W03418, doi:10.1029/2005WR004014.

Fiori, A. (2001), The Lagrangian concentration approach for determining dilution in aquifer transport: Theoretical analysis and comparison with field experiments, *Water Resour. Res.*, *37*(12), 3105–3114.

Fiori, A., and G. Dagan (2000), Concentration fluctuations in aquifer transport: A rigorous first-order solution and applications, *J. Contam. Hydrol.*, *45*(1–2), 139–163.

Fiorotto, V., and E. Caroni (2002), Solute concentration statistics in heterogeneous aquifers for finite Peclet values, *Transp. Porous Media*, *48*(3), 331–351.

Gelhar, L. W. (1993), *Stochastic Subsurface Hydrology*, Engelwood Cliffs, N.J.

Gelhar, L. W., and C. L. Axness (1983), Three-dimensional stochastic analysis of macrodispersion in aquifers, *Water Resour. Res.*, *19*, 161–180.

Grassberger, P., and I. Procaccia (1983), Characterization of strange attractors, *Phys. Rev. Lett.*, *50*(5), 346–349.

Jankovic, I., et al. (2003), Flow and transport in highly heterogeneous formations: 3. Numerical simulations and comparison with theoretical results, *Water Resour. Res.*, *39*(9), 1270, doi:10.1029/2002WR001721.

Kapoor, V., and L. W. Gelhar (1994a), Transport in three-dimensionally heterogeneous aquifers. 1. Dynamics of concentration fluctuations, *Water Resour. Res.*, *30*(6), 1775–1788.

Kapoor, V., and L. W. Gelhar (1994b), Transport in three -dimensionally heterogeneous aquifers. 2. Predictions and observations of concentration fluctuations, *Water Resour. Res.*, *30*(6), 1789–1801.

Kapoor, V., and P. K. Kitanidis (1998), Concentration fluctuations and dilution in aquifers, *Water Resour. Res.*, *34*(5), 1181–1193.

Kitanidis, P. K. (1994), The concept of the dilution index, *Water Resour. Res.*, *30*(7), 2011–2026, doi:10.1029/94WR00762.

Le Borgne, T., J.-R. de Dreuzy, P. Davy, and O. Bour (2007), Characterization of the velocity field organization in heterogeneous media by conditional correlations, *Water Resour. Res.*, *43*, W02419, doi:10.1029/2006WR004875.

Le Borgne, T., et al. (2010), Non-Fickian mixing: Temporal evolution of the scalar dissipation rate in heterogeneous porous media, *Adv. Water Resour.*, *3*(12), 1468–1475.

Le Borgne, T., et al. (2011), Persistence of incomplete mixing: A key to anomalous transport, *Phys. Rev. E*, *84*(1), 015301.

Le Goc, R., et al. (2009), Statistical characteristics of flow as indicators of channeling in heterogeneous porous and fractured media, *Adv. Water Resour.*, *33*(3), 257–269.

Neuman, S. P., and Y.-K. Zhang (1990), A quasi-linear theory of non-Fickian and Fickian subsurface dispersion. 1. Theoretical analysis with application to isotropic media, *Water Resour. Res.*, *26*(5), 887–902.

Pannone, M., and P. K. Kitanidis (1999), Large-time behavior of concentration variance and dilution in heterogeneous formations, *Water Resour. Res.*, *35*(3), 623–634.

Pope, S. (2000), *Turbulent flows*, Cambridge Univ. Press, New York.

Rolle, M., et al. (2009), Enhancement of dilution and transverse reactive mixing in porous media: Experiments and model-based interpretation, *J. Contam. Hydrol.*, *110*(3–4), 130–142.

Salandin, P., and V. Fiorotto (1998), Solute transport in highly heterogeneous aquifers, *Water Resour. Res.*, *34*(5), 949–961.

Tartakovsky, A. M., et al. (2008), Stochastic Langevin model for flow and transport in porous media, *Phys. Rev. Lett.*, *101*(4), 4.

Tennekes, H., and J. L. Lumley (1972), *A First Course in Turbulence*, MIT Press, Cambridge, Mass.

Tonina, D., and A. Bellin (2008), Effects of pore-scale dispersion, degree of heterogeneity, sampling size, and source volume on the concentration moments of conservative solutes in heterogeneous formations, *Adv. Water Resour.*, *31*(2), 339–354.

Vanderborght, J. (2001), Concentration variance and spatial covariance in second-order stationary heterogeneous conductivity fields, *Water Resour. Res.*, *37*(7), 1893–1912.

Villermaux, J., and J. C. Devillon (1972), Représentation de la coalescence et de la redispersion des domaines de ségrégation dans un fluide par un modèle d'interaction phénoménologique, in *Proceedings of the 2nd International Symposium of Chemical Reaction Engineers*, pp. 1–14, Elsevier, New York.